

**CdSe AND TiO₂ PHOTOANODE BY
ELECTROPHORETIC DEPOSITION FOR
QUANTUM DOT SENSITIZED SOLAR CELL**

HAY MAR AUNG KYAW

UNIVERSITI SAINS MALAYSIA

2020

**CdSe AND TiO₂ PHOTOANODE BY
ELECTROPHORETIC DEPOSITION FOR
QUANTUM DOT SENSITIZED SOLAR CELL**

by

HAY MAR AUNG KYAW

**Thesis submitted in fulfilment of the requirements
for the degree of
Doctor of Philosophy**

July 2020

ACKNOWLEDGEMENT

First of all, I would like to express my deepest gratitude to my main supervisor Assoc. Prof. Dr. Khatijah Aisha Yaacob and to my co-supervisor Prof. Dr. Ahmad Fauzi Bin Mohd Noor for their guidance, inspiration, devotion, patience, and perpetual encouragement throughout my doctoral study. It would not have been possible for me to bring out this thesis without their help and constant encouragement. I wish that I would keep in mind her mention that Ph.D study is just one of chapters in my life, not the end. I believe that this chapter would be the great foundation in my future. I also would like to thanks to my sincere gratitude to my co-supervisor Prof. Atsunori Matsuda from Toyohashi University of Technology (TUT) for his guidance, invaluable suggestions, and encouragement, Assoc. Prof. Dr. Go Kawamura and Dr. Tan Wai Kian from Toyohashi University of Technology (TUT) for their valuable help and supporting during my study at Japan, Prof. Dr. Aye Aye Thant from University of Yangon, Myanmar for his guidance and encouragements. I am deeply thankful to School of Materials and Minerals Resources Engineering, Universiti Sains Malaysia (USM) for offering me an opportunity to pursue Ph.D at Materials Engineering with sufficient research facilities, great supports from administrative, academic and technical staff. I am grateful to Japan International Cooperation Agency (JICA), ASEAN University Network/Southeast Asia Engineering Education Development Network (AUN/SEED-Net) for the financial support and a great opportunity for collaborative research in Matsuda-MutoKawamura laboratory, Toyohashi University of Technology (TUT) through AUN/SEED-Net project. I also would like to thanks to all of my friends at USM, TUT and Yangon University for their great companion and help when I am facing with difficulties. All activities that we had together are

unforgotten. Their friendship is a blessing, my heart will always treasure. Finally, I would like to express special gratitude to my beloved parents; U Aung Kyaw and Daw Khin Htay Yie, my sister; Daw Ohmmar Aung Kyaw for their unconditional support, motivation, and encouragement. It is impossible for me to finish this work without their encouragement and understanding. My special appreciation and gratitude to all of my brothers and their families for their unconditional love and kindness.

Thank You.

Hay Mar

TABLE OF CONTENTS

ACKNOWLEDGEMENT	ii
TABLE OF CONTENTS.....	iv
LIST OF TABLES	x
LIST OF FIGURES	xiii
LIST OF SYMBOLS	xxi
LIST OF ABBREVIATIONS	xxiii
LIST OF APPENDICES.....	xxiv
ABSTRAK.....	xxv
ABSTRACT	xxvii
CHAPTER 1 INTRODUCTION	1
1.1 Introduction.....	1
1.2 Problem Statement	9
1.3 Research Objectives	12
1.4 Research Scope	12
1.5 Organization of Thesis.....	13
CHAPTER 2 LITERATURE REVIEW	15
2.1 Introduction.....	15
2.2 CdSe Nanoparticles	16
2.2.1 Properties of CdSe Nanoparticles	16
2.2.2 Synthesis of CdSe Nanoparticles	18
2.2.3 Growth Mechanism of CdSe Nanoparticles during Synthesis.....	19
2.2.4 TOPO Ligand.....	21
2.2.5 Optical Properties of CdSe Nanoparticles	22
2.2.6 Purification of CdSe Nanoparticles Solution.....	23
2.2.7 Optical Properties of Purified CdSe Nanoparticles	26

2.2.8	Zeta Potential of Purified CdSe Nanoparticles	27
2.3	Titanium Dioxide (TiO ₂)	28
2.4	Deposition Methods of Quantum Dots (QDs)	31
2.4.1	Successive Ionic Layer Adsorption and Reaction (SILAR)	33
2.4.2	Chemical Bath Deposition (CBD)	33
2.4.3	Surface Attachment through Molecular Linkers.....	35
2.4.4	Direct Adsorption (DA).....	36
2.4.5	Electrophoretic Deposition (EPD)	36
	2.4.5(a) Mechanism of EPD	38
	2.4.5(b) Parameters Related to the Colloidal Properties of Suspension	41
	2.4.5(c) Parameters Related to the EPD Process	44
2.5	Application of EPD	47
2.6	EPD of CdSe Nanoparticles.....	49
2.7	EPD of TiO ₂ Nanoparticles.....	50
2.8	Co-Deposition of EPD.....	53
2.9	Working Principle of Quantum Dot Sensitized Solar Cells (QDSSCs)	55
2.9.1	Photoanode (Working Electrode).....	56
2.9.2	Photocathode (Counter Electrode)	58
2.9.3	Electrolyte	59
CHAPTER 3	MATERIALS AND METHODOLOGY	64
3.1	Introduction.....	64
3.2	Raw Materials and Chemicals.....	64
3.2.1	Chemicals Involved in the Synthesis of CdSe Nanoparticles Solution.....	65
3.2.2	Synthesis of CdSe Nanoparticles	65
3.2.3	Purification of CdSe Nanoparticles Solution.....	68
3.3	Preparation of TiO ₂ Nanoparticles	68

3.3.1	Chemicals Involved in the Preparation of TiO ₂ Nanoparticles.....	69
3.3.2	Preparation of Surface Modified Titanium (IV) Isopropoxide (TTIP) Using Propionic Acid and n-hexylamine (Method 1)	69
3.3.3	Preparation of Surface Modified TiO ₂ (P25, Degussa) Nanoparticles using Propionic Acid and N-Hexylamine (Method 2)	71
3.4	Chemicals Involved in the Preparation of the Photoanode and RCA Solution.....	73
3.4.1	Cleaning of Fluorine-doped Tin Oxide (FTO) Glass Using Normal and Radio Corporation of America (RCA) Processes	74
3.5	Electrophoretic Deposition (EPD).....	75
3.5.1	EPD of Single Layer CdSe	75
3.5.2	EPD of Single Layer TiO ₂	76
3.5.3	EPD of Mixed CdSe-TiO ₂	77
3.5.4	EPD of CdSe/TiO ₂	77
3.6	Chemicals and Materials Involved in the Preparation of Polysulfide Electrolyte and Copper – Brass Counter Electrode.....	78
3.6.1	Preparation of Polysulfide Electrolyte	78
3.6.2	Preparation of Copper-Brass Counter Electrode.....	79
3.7	Assembly of Quantum Dots Sensitized Solar Cell (QDSSC).....	80
3.8	Characterization Techniques	82
3.8.1	UV-Vis Spectroscopy	83
3.8.2	Zeta Potential Analysis	85
3.8.3	X-ray Diffraction (XRD) Analysis.....	87
3.8.4	Field Emission Scanning Electron Microscopy (FESEM)	89
3.8.5	Transmission Electron Microscopy (TEM)/High-Resolution Transmission Electron Microscopy (HRTEM).....	90
3.8.6	Current Density-Voltage (J-V) Measurement.....	91
3.8.7	Electrochemical Impedance Spectroscopy (EIS).....	93
CHAPTER 4 RESULTS AND DISCUSSION		96
4.1	Introduction.....	96

4.1.1	Effect of TOPO amounts in the preparation of CdSe Solution.....	97
4.1.1(a)	UV-Visible Analysis	97
4.1.1(b)	Zeta Potential.....	99
4.1.2	Purification process of CdSe nanoparticles solution prepared with different amount of TOPO.....	100
4.1.2(a)	Optical Properties of Purified CdSe Nanoparticles.....	101
4.1.2(b)	Zeta Potential for Purified CdSe Nanoparticles	102
4.1.3	Electrophoretic Deposition of CdSe Nanoparticles on Fluorine Doped Tin Oxide	103
4.2	Effect of the Purification of 8g TOPO in CdSe Nanoparticles Solution	105
4.3	XRD Analysis of TiO ₂ Nanoparticles	108
4.4	Electrophoretic Deposition of CdSe (8g, TOPO) Nanoparticles on FTO Substrate.....	111
4.4.1	Effect of Suspension Volume	112
4.4.1(a)	Zeta Potential Measurement	112
4.4.1(b)	SEM Analysis	112
4.4.2	Effect of Applied Voltage.....	115
4.4.2(a)	SEM Analysis	115
4.4.3	Effect of Deposition Time	118
4.4.3(a)	SEM Analysis	119
4.4.4	Effect of Gap between FTO Electrodes.....	121
4.4.4(a)	SEM Analysis	122
4.5	EPD of TiO ₂	125
4.5.1	EPD Parameters Related to the Processing of TiO ₂ Nanoparticles. 125	
4.5.1(a)	Concentration of TiO ₂ Nanoparticle Suspension	126
4.5.1(b)	Applied Voltage during EPD of TiO ₂ Nanoparticle Suspension	127
4.5.1(c)	Deposition Time of TiO ₂ Nanoparticle Suspension.....	129
4.5.1(d)	Effect of Gap between FTO Electrodes	132

4.6	Electrophoretic Co-deposition of CdSe-TiO ₂ Nanoparticle	134
4.6.1	EPD Parameters Related to the Processing of CdSe-TiO ₂ Nanoparticle	134
4.6.1(a)	Deposition time of mixture CdSe and TiO ₂ Nanoparticle Suspension	134
4.6.1(b)	Mixture CdSe and TiO ₂ Nanoparticle Films with Different TiO ₂ Concentration	136
4.6.1(c)	Mixture CdSe and TiO ₂ Nanoparticle Films with Different CdSe Volume	138
4.7	Layer by Layer EPD of CdSe/TiO ₂	140
4.7.1	EPD Parameters Related to the Processing of CdSe/TiO ₂ Film	140
4.7.1(a)	Effect of CdSe Deposition Time on TiO ₂ Film	140
4.7.1(b)	Effect of CdSe Applied Voltage on TiO ₂ Film	145
4.7.2	Effect of CdSe Particles Sizes on TiO ₂ Film	146
4.8	Current Density-Voltage (J-V) Measurement	153
4.8.1	Mixed CdSe and TiO ₂ Nanoparticle Films with Varying TiO ₂ Concentrations	153
4.8.2	Mixed CdSe and TiO ₂ Nanoparticle Films for Different Deposition Time	155
4.8.3	Mixed CdSe and TiO ₂ Nanoparticle Films for Different CdSe Volume	156
4.8.4	J-V curve of QDSSC with CdSe/TiO ₂ Films for Different Deposition Times	158
4.8.5	J-V curve of QDSSC with CdSe/TiO ₂ Films for Different Applied Voltages	160
4.8.6	J-V Curve for QDSSC with Different CdSe Particles Sizes	162
4.9	Electrochemical Impedance Spectroscopy (EIS) Measurements	163
4.9.1	Mixed CdSe and TiO ₂ Nanoparticle Films with Different Deposition Times	164
4.9.2	Mixed CdSe and TiO ₂ Nanoparticle Films with Varying TiO ₂ Concentration	165
4.9.3	QDSSC of Mixed CdSe and TiO ₂ Nanoparticle Films for Varying CdSe Volume	167

4.9.4	CdSe Deposited on TiO ₂ Films with Different Deposition Times..	169
4.9.5	CdSe Deposited on TiO ₂ /FTO Films with Different Applied Voltages	171
4.9.6	Different CdSe Particles Sizes on TiO ₂ Film.....	173
CHAPTER 5 CONCLUSION AND FUTURE RECOMMENDATIONS .		175
5.1	Conclusion	175
5.2	Recommendations for Future Research.....	179
REFERENCES		180
APPENDICES		
LIST OF PUBLICATIONS		

LIST OF TABLES

	Page
Table 2.1 List of the stability behavior of the colloid suspension in relation to zeta potential (Riddick, 1968).	43
Table 2.2 Summary of nanoparticles for QDSSCs	61
Table 2.3 Summary of counter electrodes for QDSSCs.....	62
Table 2.4 Summary of electrolytes for QDSSCs	63
Table 4.1 The wavelength absorbance and particles size values of non-purification CdSe nanoparticles solutions with different concentration of TOPO.	98
Table 4.2 Zeta potential of different concentration of TOPO in CdSe nanoparticles solutions for non- purified conditions.	100
Table 4.3 The wavelength and absorbance values of CdSe nanoparticles solutions for 1 × cycle purification.	102
Table 4.4 Zeta potential of different concentration of TOPO in CdSe nanoparticles solutions for 1 × cycle purification.	103
Table 4.5 Zeta potential and conductivity values of 8g TOPO in CdSe solution through 4 × cycles purification.	107
Table 4.6 The thickness of CdSe deposited on FTO films at 100 V for 60 seconds and 2 mm gaps with the different volume CdSe solution. .	115
Table 4.7 The thickness of CdSe deposited on FTO films at different applied voltages for 60 seconds and 2 mm gaps.....	117
Table 4.8 The thickness of CdSe deposited on FTO films at different deposition times at 200 V and 2-mm gap.	120
Table 4.9 The thickness of CdSe deposited on FTO films at different electrodes gaps at 200 V for 30 seconds.	124

Table 4.10	The thickness of TiO ₂ deposited on FTO films at 150 V for 30 seconds and 2 mm gaps with the different TiO ₂ suspension concentration.	127
Table 4.11	The thickness of 3 mg/ml concentration TiO ₂ deposited on FTO films at different applied voltages for 30 seconds and 2 mm gaps..	129
Table 4.12	The thickness of 3 mg/ml concentration TiO ₂ deposited on FTO films at different deposition times at 150 V- and 2-mm gaps.	131
Table 4.13	The thickness of 3 mg/ml concentration TiO ₂ deposited on FTO substrate at different electrodes gaps at 150 V for 30 seconds.	133
Table 4.14	J-V results for mixed CdSe and TiO ₂ films with Varying TiO ₂ Concentration	155
Table 4.15	J-V results for mixing CdSe and TiO ₂ films.	156
Table 4.16	J-V results for mixing CdSe and TiO ₂ films with Varying CdSe Concentration	157
Table 4.17	J-V results for CdSe/TiO ₂ films with CdSe deposition times.	160
Table 4.18	J-V results for CdSe/TiO ₂ films with CdSe applied voltages.	161
Table 4.19	J-V results for CdSe (2.5 nm)/TiO ₂ and CdSe (3.2 nm)/TiO ₂ films.	163
Table 4.20	Electrochemical properties of QDSSC with CdSe-TiO ₂ Films of different deposition times.....	164
Table 4.21	Series resistance and efficiency values for EIS spectra of CdSe-TiO ₂ films with different deposition times.....	166
Table 4.22	Series resistance and efficiency values for EIS spectra of CdSe-TiO ₂ films with different deposition times.....	168
Table 4.23	Series resistance and efficiency values for EIS spectra of CdSe/TiO ₂ films with different deposition times.	171
Table 4.24	Series resistance and efficiency values for EIS spectra of CdSe-TiO ₂ / films with different deposition times.....	173

Table 4.25	Series resistance and efficiency values for EIS spectra of different CdSe nanoparticles sizes on TiO ₂ Films.	174
------------	---	-----

LIST OF FIGURES

	Page
Figure 1.1 Shows the efficiency chart by NREL, to compare all the three-generation solar cell.	3
Figure 1.2 Schematic diagram illustrating the energy levels of different-sized CdSe QDs and TiO ₂	5
Figure 1.3 Structure and operating principle of a typical QDSSC (Jun et al., 2013).	9
Figure 2.1 Different sizes CdSe quantum dots, synthesized at a slow-increasing temperature gradient with different color light emissions (A) images under UV irradiation and on visible light (B) normalized absorbance spectra (Zlateva et al., 2007).	16
Figure 2.2 Energy level diagram of CdSe nanoparticles (Vinitha & Divya, 2018).	17
Figure 2.3 Growth of CdSe nanoparticles onto TOPO matrix (Geissbühler, 2005).	20
Figure 2.4 Stages of growth and nucleation of quantum dots based on La Mer model (Farkhani and Valizadeh, 2014).	20
Figure 2.5 Schematic diagram of charge transferring at the interfacial region in QDSSC based on colloidal CdSe QDs capped by (a) long organic chain, oleate; and (b) atomic level inorganic ligand, S ²⁻ (Yun et al., 2014).	21
Figure 2.6 Absorption spectra and photoluminescence spectra of different sized CdSe quantum dots (Yuan and Krüger, 2011).	23
Figure 2.7 Chemical structure of ligands present after the synthesis of CdSe QDs (Morris-Cohen et al., 2010).	25
Figure 2.8 Schematic diagram of the effect of purification steps on the CdSe QDs surface (Morris-Cohen et al., 2010).	25

Figure 2.9	Absorption spectra change of nanoparticles as a function of purification steps (Kalyuzhny and Murray, 2005).....	26
Figure 2.10	UV-vis spectra of CdSe QDs as a function of purification steps (PS1-PS-4) (Morris-Cohen et al., 2010).	27
Figure 2.11	Zeta potential and mobility distribution of (a) 3.2 nm CdSe nanoparticles and (b) 2.3 nm CdSe nanoparticles as a function of washing cycles (Jia et al., 2008).	28
Figure 2.12	Various approaches of depositing a QD suspension on electrode surfaces: (a) drop casting or spin coating, (b) CBD, (c) SILAR, (d) electrophoretic deposition, and (e) a bifunctional linker approach (Kamat, 2013).....	32
Figure 2.13	Schematic diagram of an electrophoretic deposition process (Sarkar and Nicholson, 1996).....	37
Figure 2.14	Schematic diagram of the electrical double layer (EDL) distortion and thinning mechanism for electrophoretic deposition (Sarkar and Nicholson, 1996).	41
Figure 2.15	Relationship between deposit thickness and time of deposition for ZnO coating on copper electrode at different applied potentials (Zinc & Coatings 2004).	45
Figure 2.16	Operation mechanism of a QDSSC, with band levels, energy levels, flow of electrons, and hole (Jun et al. 2013).	56
Figure 3.1	Flowchart of the CdSe nanoparticles preparation.....	67
Figure 3.2	Schematic diagram of the CdSe purification process.	68
Figure 3.3	Flowchart of the preparation of TiO ₂ nanoparticles.	71
Figure 3.4	Flowchart of the preparation TiO ₂ (P25) nanoparticles.	73
Figure 3.5	Schematic diagram of electrophoretic deposition of charged particles on the anode and cathode of an EPD cell with planar electrodes.....	76
Figure 3.6	(a) Electrodes and (b) setup for the electrophoretic deposition process.....	76

Figure 3.7	Heating profile for thermal annealing of TiO ₂ films.	78
Figure 3.8	(a) Polysulfide electrolyte solution and (b) conductivity test for the polysulfide electrolyte solution.	79
Figure 3.9	Brass plate condition before and after immersion into HCl: (a) Normal brass plate, (b) Brass plate turns into dark red colour after immersion into HCl at 70 °C for 1 hour and (c) Formation of Cu ₂ S counter electrode after adding polysulfide solution.....	80
Figure 3.10	Flowchart of sample preparation and characterization steps for QDSSCs.	81
Figure 3.11	Assembly of QDSSC using CdSe/TiO ₂ photoanode and brass/Cu ₂ S as the counter electrode.....	82
Figure 3.12	Image of dip cell and quartz cuvette for zeta potential measurement.....	87
Figure 3.13	QDSSCs under illumination from the compact xenon lamp.....	91
Figure 3.14	Current–voltage curve of a photovoltaic solar cell under dark and ...	92
Figure 3.15	(a) Equivalent circuit used to fit the EIS spectra and (b) A Nyquist plot showing all resistive elements.	95
Figure 4.1	UV-Visible absorption spectra of non-purified CdSe nanoparticles with amounts of (a) 2g (b) 4g (c) 6g (d) 8g (e) 10g TOPO and (b) graph of wavelength vs amount of TOPO.....	99
Figure 4.2	Plot of $(\alpha h\nu)^2$ versus $h\nu$, illustrates the dependency of the crystal size on the energy band gaps of the prepared CdSe nanoparticles for different amounts of TOPO	99
Figure 4.3	(a) UV-Visible absorption spectra of CdSe nanoparticles with different amount of TOPO for 1 × cycle purification (b) The graph of wavelength before and after purification.	102
Figure 4.4	Images of CdSe films with different amount of TOPO (a) 2g (b) 4g (c) 6g (d) 8g and (e) 10g.	105
Figure 4.5	Particle distribution of CdSe (8g TOPO) nanoparticles and inset of the HRTEM images of CdSe (8g TOPO) nanoparticles.	105

Figure 4.6	UV-Visible absorption spectra of 8g TOPO in CdSe nanoparticles through 4 × cycles purification.....	107
Figure 4.7	XRD TiO ₂ nanoparticles prepared by Method (1) (A = anatase).	110
Figure 4.8	XRD TiO ₂ nanoparticles prepared by Method (2) (R = Rutile).	110
Figure 4.9	(a) HR-TEM and (b) SAED pattern of TiO ₂ nanoparticles prepared by method (1).	110
Figure 4.10	(a) HR-TEM and (b) SAED pattern of TiO ₂ nanoparticles prepared by method (2).	111
Figure 4.11	Conduction band and valence band levels of TiO ₂ (a) method (1) and (b) method (2).	111
Figure 4.12	Zeta potential values of CdSe nanoparticles solutions for varying volume.....	112
Figure 4.13	Images of CdSe deposited on FTO for different CdSe suspension volumes (a) 1 (b) 3 (c) 5 (d) 7 and (e) 10 ml at 100 V for 60 seconds.	113
Figure 4.14	SEM images for CdSe deposited on FTO at suspension volumes of (a) 3 (b) 5 (c) 7 (d) 10 ml at 100 V for 60 seconds and 2 mm gap. .	114
Figure 4.15	Images of 10 ml CdSe deposited on FTO at different applied voltage of (a) 100 V (b) 150 V (c) 200 V (d) 250 V (e) 300 V for 60 seconds and 2 mm gap.	116
Figure 4.16	SEM images for 10 ml CdSe deposited on FTO at different applied voltage of (a) 100 V (b) 150 V (c) 200 V (d) 250 V (e) 300 V for 60 seconds and 2 mm gap.	118
Figure 4.17	Images of 10 ml CdSe deposited on FTO at different deposition times of (a) 30 (b) 60 (c) 90 (d) 120 (e) 150 seconds at 200 V, and 2 mm gap.....	119
Figure 4.18	SEM images for 10 ml CdSe deposited on FTO at different deposition times of (a) 30 (b) 60 (c) 90 (d) 120 (e) 150 seconds at 200 V, and 2 mm gap.	121

Figure 4.19	Images of 10 ml CdSe deposited on FTO at different electrodes gaps of (a) 2 mm (b) 4 mm (c) 6 mm (d) 8 mm (e) 10 mm at 200 V for 30 seconds.	122
Figure 4.20	SEM images for 10 ml CdSe deposited on FTO at different electrodes gaps of (a) 2 (b) 4 (c) 6 (d) 8 and (e) 10 mm at 200 V for 30 seconds.	123
Figure 4.21	An illustration of CdSe deposition using EPD at (a) 2 mm (small gap) and (b) 8 mm (larger gap) of electrodes.	125
Figure 4.22	SEM images for TiO ₂ deposited on FTO at suspension concentrations of (a) 3 (b) 4 (c) 5 mg/ml at 50 V for 30 seconds. ..	127
Figure 4.23	SEM images for 3 mg/ ml TiO ₂ deposited on FTO at different applied voltage of (a) 50 (b) 100 (c) 150 and (d) 200 V for 30 seconds.	129
Figure 4.24	SEM images for 3 mg/ ml TiO ₂ deposited on FTO at deposition times of (a) 30 (b) 40 (c) 50 (d) 60 (e) 70 seconds at 150 V.	131
Figure 4.25	SEM images for 3 mg/ ml TiO ₂ deposited on FTO at different electrode gaps of (a) 2, (b) 4, (c) 6, (d) 8, and (e) 10 mm at applied voltage 150 V for 30 s deposition time.	133
Figure 4.26	SEM images of deposition time of mixed CdSe (5 ml) and TiO ₂ (3 mg/ml) films at 100 V applied voltage and (a) 30, (b) 60, and (c) 90-seconds deposition time.	135
Figure 4.27	Thickness vs. deposition time of mixed CdSe and TiO ₂ nanoparticles at applied voltage 100 V for 30, 60, and 90 seconds.	135
Figure 4.28	SEM images of mixture CdSe (5 ml) and TiO ₂ films with varying TiO ₂ concentration (a) 1, (b) 2, (c) 3, (d) 4, and (e) 5 mg/ml at 100 V applied voltage for 30 seconds deposition time.	137
Figure 4.29	Thickness vs. TiO ₂ for different concentration in the mixture of CdSe and TiO ₂ nanoparticles at applied voltage of 100 V for 30 seconds deposition time.	137

Figure 4.30	SEM images of mixture CdSe and TiO ₂ (3 mg/ml) films with varying CdSe volume (a) 1, (b) 3, (c) 5, (d) 7, and (e) 10 ml at 100 V applied voltage for 30 seconds deposition time.....	139
Figure 4.31	Thickness vs. for different volume of CdSe in mixed of CdSe and TiO ₂ nanoparticles at applied voltage of 100 V for 30 seconds deposition time.	139
Figure 4.32	SEM images of CdSe nanoparticles deposited on TiO ₂ layer (a) 60, (b) 90, and (c) 120 s at applied voltage 100 V and electrode gap 2 mm.	141
Figure 4.33	Thickness vs. deposition time of CdSe nanoparticles deposited on TiO ₂ film.	141
Figure 4.34	(a) Schematic diagram of CdSe/TiO ₂ based QDSSC and (b).....	143
Figure 4.35	UV-vis absorption spectra of (a) TiO ₂ and different deposition time of CdSe (b) 60, (c) 90, and (d) 120 seconds on TiO ₂ films at 100 V.....	144
Figure 4.36	Band gap of (a) TiO ₂ and (b) different deposition time of CdSe (a) 60, (b) 90, and (c) 120 seconds on TiO ₂ films at 100 V.	144
Figure 4.37	SEM images of (a) CdSe (100V, 120s)/ TiO ₂ (150 V, 30s) (b) CdSe (120V, 120s)/ TiO ₂ (150 V, 30s) (c) CdSe (150V, 120s)/ TiO ₂ (150 V, 30s) films.	146
Figure 4.38	Thickness vs. applied voltage of CdSe nanoparticles deposited on TiO ₂ film.	146
Figure 4.39	(a) CdSe (2.5 nm)/TiO ₂ (b) CdSe (3.2 nm)/TiO ₂ films.....	147
Figure 4.40	UV-vis spectra of (a) TiO ₂ (b) CdSe (2.5 nm)/TiO ₂ (c) CdSe (3.2 nm)/TiO ₂ films.....	148
Figure 4.41	SEM images of (a) CdSe (2.5 nm)/TiO ₂ (b) CdSe (3.2 nm)/TiO ₂ films.	149
Figure 4.42	The surface morphology of SEM images for (a) CdSe (2.5 nm)/TiO ₂ (b) CdSe (3.2 nm)/TiO ₂ films.	150

Figure 4.43	(a) TEM image of CdSe (2.5 nm)/TiO ₂ and corresponding EDS mapping images of (b) Ti (c) O (d) Cd (e) Se and (f) EDS spectrum.	150
Figure 4.44	(a) STEM image of CdSe (3.2 nm)/TiO ₂ and corresponding EDS mapping images of (b) Ti (c) O (d) Cd (e) Se and (f) EDS spectrum	152
Figure 4.45	J-V curves of fabricated QDSSCs using mixed CdSe (5 ml) and TiO ₂ with different concentration (a) 1, (b) 2, (c) 3, (d) 4, and (e) 5 mg/ml films under AM 1.5 G illumination (100 mW/cm ²).	154
Figure 4.46	J-V curves of QDSSCs fabricated using mixed CdSe and TiO ₂ (a) 100V, 30s (b) 100V, 60s and (c) 100V, 90s films under AM 1.5 G illumination (100 mW/ cm ²).....	156
Figure 4.47	J-V curves of QDSSCs fabricated using mixing CdSe and TiO ₂ with CdSe different volume (a) 1, (b) 3, (c) 5, (d) 7, and (e) 10 ml films under AM 1.5 G illumination (100 mW/cm ²).	158
Figure 4.48	J-V curves of QDSSCs fabricated using CdSe/TiO ₂ films with different CdSe deposition times under AM 1.5 G illumination (100 mW/cm ²).	159
Figure 4.49	J-V curves of QDSSCs fabricated using (a) CdSe (100V, 120s)/TiO ₂ (b) CdSe (120V, 120s)/TiO ₂ (c) CdSe (150V, 120s)/TiO ₂ films under AM 1.5 G illumination (100 mW/cm ²).	161
Figure 4.50	J-V curves of QDSSCs fabricated using 2.5 nm and 3.2 nm particles sizes of CdSe QDs on TiO ₂ films under AM 1.5 G illumination (100 mW /cm ²).....	163
Figure 4.51	Nyquist plot for CdSe-TiO ₂ Films with (a) 30, (b) 60, and (c) 90 seconds deposition time.	165
Figure 4.52	Nyquist plots for CdSe-TiO ₂ films with different TiO ₂ concentration (a) 1 (b) 2 (c) 3 (d) 4 (e) 5 mg/ml at 100 V applied voltage for 30seconds deposition times.	167

Figure 4.53	Nyquist plots for mixed QDSSC with CdSe and TiO ₂ (3 mg/ml) films with varying CdSe volume (a) 1 (b) 3 (c) 5(d) 7 and (e) 10 ml at 100 V applied voltage for 30 seconds deposition time.	169
Figure 4.54	Nyquist plots for CdSe deposited on TiO ₂ films with (a) 60 (b) 90 (c) 120 seconds deposition times at 100 V applied voltage.	171
Figure 4.55	Nyquist plots for CdSe deposited on TiO ₂ films with (a) 100 (b) 120 (c) 150 applied voltage for 120 seconds deposition times.	172
Figure 4.56	Extracted parameter plots from EIS measurement of QDSSCs (a) CdSe (2.5 nm)/TiO ₂ (b) CdSe (3.2 nm)/TiO ₂ Nyquist plots.	174

LIST OF SYMBOLS

%	Percentage
°	Degree
°C	Degree Celsius
ml	Milliliter
wt%	Weight percentage
V	Voltage
g	Gram
h	Hour
s	Second
h ν	Photon energy
2θ	Diffraction angle
nm	Nanometer (10^{-9} m)
μm	Micrometer (10^{-6} m)
β	Full-width at half-maximum (radius)
C	Capacitance
η	Photoconversion efficiency
h^+	Holes
λ	Wavelength
α	Absorption coefficient
D	Crystallite size
Z'	Real impedance
Z''	Imaginary impedance
R_s	Series resistance
R_{ct}	Charge transfer resistance
f	Frequency

ϵ	Dielectric constant
I	Current
J_{\max}	Current density at maximum power point
V_{\max}	Voltage at maximum power point
J_{sc}	Photocurrent density at short circuit
V_{oc}	Open circuit voltage
P_{in}	Intensity of the incident light
E_{g}	Band gap energy
h	Plank's constant

LIST OF ABBREVIATIONS

CB	Conduction Band
VB	Valence Band
DA	Direct Absorption
CE	Counter Electrode
FTO	Fluorine Doped Tin Oxide
EIS	Electrochemical Impedance Spectroscopy
J-V	Current Density-Voltage
UV-vis	UV-Visible Spectroscopy
QDSSC	Quantum Dots Sensitized Solar Cell
DSSC	Dye Sensitized Solar Cell
HRTEM	High Resolution Transmission Electron Microscopy
EPD	Electrophoretic Deposition
QD	Quantum Dot
SILAR	Successive Ionic Layer Adsorption and Reaction
CBD	Chemical Bath Deposition
DA	Direct Adsorption
CQD	Colloidal Quantum Dot Solar Cell
EDL	Electrical Double Layer
FF	Fill Factor
XRD	X-Ray Diffraction
RCA	Radio Corporation of America

LIST OF APPENDICES

- APPENDIX A THE CONDUCTIVITY OF THE SUSPENSION VALUES
- APPENDIX B THE CALCULATION EQUATION OF THE ENERGY BAND
GAP, CONDUCTION BAND, AND VALENCE BAND OF
TiO₂ AND CdSe

FOTOANOD CDSE AND TiO₂ MENGGUNAKAN PEMENDAPAN ELECTROFORESIS BAGI SEL SOLAR DOT KUANTUM TERPEKA

ABSTRAK

Nanopartikel CdSe telah digunakan sebagai pemeka foton di dalam sel solar terpeka berkuantum dot (QDSSC). Dalam kajian ini, nanopartikel CdSe telah disintesis menggunakan kaedah pancutan hangat dengan jumlah ligan TOPO yang berbeza. Nanopartikel CdSe diserakan di dalam kloroform berikutan proses penulenan. 8 g TOPO CdSe telah digunakan dalam proses pemendapan. CdSe dimendapkan kepada substrat tin oksida terdop fluorin (FTO) menggunakan kaedah pemendapan elektroforesis (EPD) dengan parameter yang berbeza. CdSe dimendapkan kepada saput TiO₂ manakala campuran CdSe-TiO₂ dimendapkan kepada substrat FTO. Nanopartikel TiO₂ telah berjaya disediakan melalui pengubahsuaian menggunakan asid propionik dan n-heksilamina dengan melarutkan nanopartikel TiO₂ di dalam kloroform. TiO₂ dimendapkan kepada substrat tin oksida terdop fluorin (FTO) menggunakan kaedah pemendapan elektroforesis (EPD) dengan parameter yang berbeza. Bagi saput CdSe/TiO₂, TiO₂ pertama sekali dimendapkan kepada FTO sebelum dipanaskan pada suhu 450 °C selama 3 jam. Seterusnya, CdSe dimendapkan kepada saput TiO₂ panas. Bagi saput campuran CdSe-TiO₂, CdSe dan TiO₂ telah dicampur dan dimendapkan kepada substrat FTO. Saput CdSe/TiO₂ dan saput campuran CdSe-TiO₂ telah disediakan menggunakan kaedah EPD sebagai fotoanod. Bagi QDSSC, saput CdSe/TiO₂ dan saput campuran CdSe-TiO₂ telah digunakan sebagai fotoanod dan kuprum (II) sulfida (Cu₂S) yang bertindak sebagai elektrod penyangkal telah digunakan di dalam elektrolit polisulfida. Kesemua fotoanod, elektrod penyangkal dan elektrolit telah dipasang bagi penilaian I-V dan

EIS. Kecekapan tertinggi bagi saput CdSe/TiO₂ adalah sebanyak 2.1% manakala bagi campuran CdSe-TiO₂ sebanyak 0.04%. Daripada hasil penilaian EIS, nilai R_{ct} bagi saput berlapis CdSe/TiO₂ dan saput campuran CdSe-TiO₂ adalah masing-masing 51 Ω dan 75 Ω . Oleh itu, saput berlapis CdSe/TiO₂ menghasilkan kecekapan yang lebih tinggi berbanding saput campuran CdSe-TiO₂ di dalam penggunaan QDSSC.

CDSE AND TiO₂ PHOTOANODE BY ELECTROPHORETIC DEPOSITION FOR QUANTUM DOT SENSITIZED SOLAR CELL

ABSTRACT

CdSe nanoparticles were used as a photon sensitizer in quantum dot sensitized solar cell (QDSSC). Mesoporous structure is desired for TiO₂ wide band gap semiconductors to provide large surface area for absorption of more QDs in harvesting visible light efficiency. Common method to make QDSSC is to couple the CdSe with TiO₂ for charge transfer. But, the problem with this system is that photoexcited electron needs to travel a long pathway (the thickness of TiO₂) before it reaches the conductive substrate, where the photoexcited electron is susceptible to recombination with the sub-band gap state of TiO₂. Mixed CdSe-TiO₂ photoanodes will create efficient electron injection from CdSe conduction band to the TiO₂ electrode effectively in order to reduce the recombination and improve the efficiency. In this research, CdSe nanoparticles were synthesized by hot injection method and using different amount of TOPO ligand. CdSe nanoparticles were dispersed in chloroform after purification process. 8 g TOPO amount of CdSe were used for deposition process. CdSe was deposited on fluorine doped tin oxide (FTO) substrate by using electrophoretic deposition method (EPD) with various EPD parameters. CdSe was deposited on TiO₂ film and mixed CdSe-TiO₂ were deposited on FTO substrate. TiO₂ nanoparticles were successfully prepared by modification using both propionic acid and n-hexylamine and TiO₂ nanoparticles dissolved in chloroform. TiO₂ was deposited on fluorine doped tin oxide (FTO) substrate by using electrophoretic deposition method (EPD) with various EPD parameters. For CdSe/TiO₂ film, TiO₂ was deposited on FTO first then this film was heated 450 °C for 3 hours. Then, CdSe was deposited

on heated TiO₂ film. For mixed CdSe-TiO₂ films, CdSe and TiO₂ was mixed together and deposited on FTO substrate. CdSe/TiO₂ film and mixed CdSe-TiO₂ film were prepared by EPD method as photoanode. For QDSSC, CdSe/TiO₂ film and mixed CdSe-TiO₂ film was used as photoanode, copper (II) sulfide (Cu₂S) as counter electrode and was used polysulfide electrolyte. These photoanode, counter electrode and electrolyte were assembled for I-V and EIS measurements. The highest efficiency of CdSe/TiO₂ film was 2.1% and 0.04% for the mixed CdSe-TiO₂ films. From the result of EIS measurement, the R_{ct} value of CdSe/TiO₂ films and mixed CdSe-TiO₂ films were 51 Ω and 75 Ω. Thus, the CdSe/TiO₂ films produced higher efficiency than mixed CdSe-TiO₂ films in QDSSC application.

CHAPTER 1

INTRODUCTION

1.1 Introduction

Rapid depletion of non-renewable energy resources, and over exploitation of conventional fossil fuels has aggravated the problems of global warming and climate change. Renewable energy has been a global issue and the demand for it has increased because of issues associated with the conversion of fossil fuel to electricity. When fossil fuels are converted to electricity, the process often result in harmful side effects such as pollution that threatens human health, and the release of greenhouse gases associated with climate change. Therefore, global research attention has been driven towards alternative, renewable, and clean energy sources such as wind, solar, tide, biomass, and biofuel (Abolhosseini et al. 2014). Although there are several potentially renewable sources of energy, solar energy is considered as a more desirable source of energy. In fact, it has attracted much attention and interest as an environment friendly energy alternative of the future which could help to prevent global warming, weather change and greenhouse effect.

The earth gets about 4.3×10^{20} of energy from sun in just one hour. This value is enough for the solar cells to harvest the sunlight and transfer the light directly into electricity without the evolution of carbon dioxide, since the planet needs only about 4.1×10^{20} J of energy per year (Lewis et al. 2005). Besides, the electric energy obtained from solar cells is clean. Based on this, a wide range of solar cell technologies are currently being developed. Some of the notably types of solar cells are dye-sensitized solar cells (Grätzel 2003), bulk heterojunction solar cells (Blom et al. 2007), depleted heterojunction solar cells (Pattantyus-Abraham et al. 2010), and hybrid organic-inorganic solar cells (Chandrasekaran et al. 2011).

In the development of solar cells, the technology has progressed in a way that they can be categorized into three generations - first, second and third generation (Werner 2004). The first-generation solar cells or photovoltaic cells are based on a single crystalline silicon wafer, while the second-generation solar cells or photovoltaic solar cells utilizes the inorganic thin film structure in the cell assembly. The second-generation solar cells are cheaper to produce compared to the single junction crystalline photovoltaic cell of the first generation. However, the efficiency of the amorphous thin film solar cells i.e., 14% is lower than the efficiency inherent in the single junction crystalline photovoltaic cell of the first generation which can go as high as 27%. Theoretically, single junction cells should be able to exhibit a maximum efficiency of ~33%, a limit set by Shockley-Queisser thermodynamics.

However, profitable commercialization of the solar cell technology is aimed at achieving efficiencies greater than 33% at lower production costs. The onset of this breakthrough is the third-generation photovoltaic cells. In the third-generation photovoltaic cells, higher efficiency devices were possible at lower production cost. Dye-sensitized solar cells (DSSCs), quantum dot-sensitized solar cells (QDSSCs), colloidal quantum dot solar cells (CQD) and organic solar cells are notable types that were developed under the third-generation solar cells or photovoltaic cells. Over the last ten years, the improvements in DSSCs has maintained the highest record ever reported, which is 12% (Jun et al. 2013; Choi et al. 2013).

At the beginning, dye-sensitized solar cells (DSSCs) with inorganic ruthenium-based dyes were made available at a low-cost and established as high-efficiency solar cells in the early 90s (Oregan & Gratzel 1991). Subsequently, numerous researches have focused on the development and characterization of different dyes for application

in DSSCs (Noor et al. 2011). In one of the developments, the QDSSC solar cells in which the dye is replaced with inorganic quantum dot (QD) nanoparticles were developed (Nozik 2002). The quantum dot was based on the DSSC's structure and used as an effective substitute to the dye due to its excellent opto-electronic properties (Grätzel 2003). Hence, quantum dot sensitized solar cells (QDSSCs) have been drawing much attention as third generation solar cells. Being semiconductor nanoparticles, the physical and chemical properties of the QDs are size-dependent. The QDs are especially appealing owing to their high extinction coefficients compared to the conventional dyes. Therefore, the attractive properties of the quantum dots solar cells revolve around the salient characteristics, such as tunability band gap of the sensitizers which offers the possibility of efficiently converting visible light to electric energy (Kamat 2008). In addition, it exhibits narrow emission spectrum, good photostability (Salant et al. 2010), broad excitation spectra, high extinction coefficient and multiple exciton generation (Quantum et al. 2010). Particularly, the ability of QDs to produce multiple exciton generation where a single absorbed photon can generate more than one electron hole-pair is fascinating. Figure 1.1 shows the efficiency chart by NREL, to compare all the three-generation solar cells.

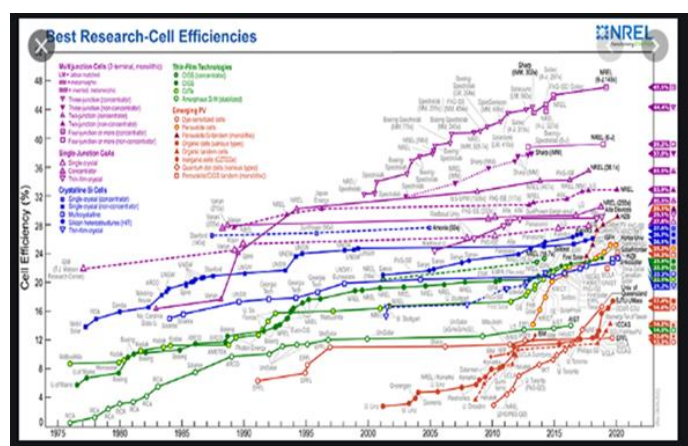


Figure 1.1 Shows the efficiency chart by NREL, to compare all the three-generation solar cell.

In recent times, cadmium chalcogenide (CdX , $\text{X} = \text{S}, \text{Se}, \text{Te}, \text{etc.}$) QDs have attracted more attention in QDSSC research. The widespread research activities taking place currently on CdX QDs are due to their distinct properties, such as ease of fabrication, tunability of band gap energy through size control and possible multiple exciton generation as stated earlier. It has been observed that CdX absorbs photon efficiently because it has a bulk material band gap above 1.3 eV (band gap for CdS , CdSe and CdTe are 2.25 eV, 1.73 eV and 1.49 eV respectively) (Peter 2011). Among these materials, CdSe is the most widely studied, mainly due to its easy synthesis, stability, and good performance in sensitized devices. In addition, CdSe has a wider absorption range ($< \text{ca. } 720 \text{ nm}$) which is in the range of greatest solar irradiances, 300-800 nm. This makes CdSe more advantageous as light harvesting nanoparticles. CdSe is one of the most important materials from group II-VI semiconductors, CdSe being the n-type semiconductor with the wurtzite crystal structure for both bulk material and nanoparticles. When the particle size of the CdSe is smaller than or comparable to its exciton Bohr radius of 5.8, the band gap increases with decreasing particle size due to the quantum confinement effect. Hence, CdSe QDs can be used as coating layers, light absorbers and as a stabilizer for the solar cell when it is coupled with wide band gap semiconductor. The CdSe QDs is stable with polysulfide electrolyte and as a result, several attempts have been made to study the combined deposition of CdSe QDs onto TiO_2 mesoporous photoanode with polysulfide as the electrolyte, to fabricate quantum dots sensitized solar cells.

In the QDSSC, the excited electrons in CdSe QDs, which absorb light in the visible range, can be transferred from the CdSe conduction band (CB) to the TiO_2 conduction band (CB). By tuning the particles size of the CdSe through quantization effect, the charge separation and the energies at the band edges can be optimized (Jun

et al. 2013). Kongkanand and co-workers reported that by varying the size of CdSe QDs assembled on TiO₂ films, improvement in photoelectrochemical response and photoconversion efficiency can be achieved. Figure 1.2. shows that with the decrease of CdSe particle size, photocurrent increases due to the shift of the CB to a more negative potential. This in turn increases the driving force for charge injection and the electron charge transfer rate increases from CdSe quantum dots to TiO₂ nanoparticles.

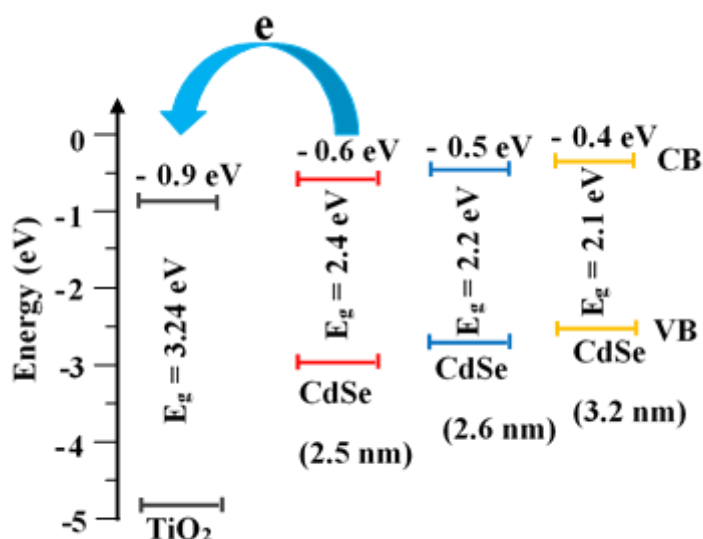


Figure 1.2 Schematic diagram illustrating the energy levels of different-sized CdSe QDs and TiO₂.

The creation of thin films of TiO₂ nanoparticles is of particular interest to scientists and industry due to its properties and its variety of potential applications. For instance, TiO₂ is the preferred material for semiconductors due to its photocatalytic activity, chemical stability, nontoxicity, and low cost compared to other materials. Additionally, TiO₂ is known to exhibit other important properties including large band gap, high electric resistivity, a high dielectric constant, and high oxidative power. These properties make it suitable to be used as capacitors in microelectronic devices, gas sensors, quantum dot synthesized solar cells, dye-based solar cells, optical filters,

antireflection coatings, and sterilization materials (Viana et al. 2010). To create these thin films with TiO₂ nanoparticles, two major processes must be employed. The first process involves the creation of nanoparticles that have the desired shape and properties needed for their intended use. The second process is to create the films of these particles through deposition. For both major processes, there are numerous methods to achieve the desired result.

There are various methods to synthesize nanostructured TiO₂. The notable methods include hydrothermal method (Andersson & Lars 2002), solvothermal method (Wahi et al. 2006), sol-gel method (Bazargan et al. 2012), direct oxidation method (Ryu et al. 2008), chemical vapor deposition (CVD) (Shinde & Bhosale 2008), sonochemical method (Arami et al. 2007), and microwave method (Ferrari et al. 2005). However, among these methods, sol-gel method is seen as a relatively simple approach which can produce highly crystalline anatase TiO₂ nanoparticles with different sizes and shapes. In another vein, there are several reports on the deposition of TiO₂ for QDSSC photoanode, such as through spin coating method (Chou et al. 2011), liquid-phase deposition techniques (Deng et al. 2016), screen printing (Abdul et al. 2017), doctor bladed (Deng et al. 2015), spray pyrolysis (Esparza et al. 2015), electrodeposition (Tan et al. 2009), and sputtering (Li et al. 2012). Notwithstanding, the scope of this study is limited to the particle synthesis through the sol-gel process, and the creation of films using electrophoretic deposition.

Notably, the unique crystal structure, photocatalytic activity, and photoluminescence properties of titanium dioxide nanoparticles are largely responsible for its various applications. Specifically, titanium dioxide is found to have three prominent crystal phases: anatase, rutile, and brookite. In nature, the most found crystal phase is rutile due to its stability. However, due to temperatures most

commonly used in the heating process during nanoparticle synthesis, the anatase phase becomes the most stable (Chen & Mao 2007). Considering that the anatase and rutile phases are the most used phases in the preparation of suspensions for electrophoretic deposition, only the properties and synthesis of these two phases will be analysed in this research.

Salant et al. reported the TiO₂ nanoparticles deposited on FTO (Salant et al. 2010b) and Chiang et al. reported the TiO₂ nanoparticles deposited on TCO through EPD method for QDSSC (Chiang et al. 2015). Likewise, Chen et al. fabricated TiO₂ photoanode on FTO through EPD method for DSSC (Chen et al. 2011). The TiO₂ nanoparticle films composed of large particles which led to higher conversion efficiencies in QDSSCs. This is because a more open structure of the TiO₂ layer facilitates the transport of QDs prior to adsorption, leading to higher QD loadings. In turn, the blockage of nanochannels (mesopores), which could make some parts of the electrode inactive, is prevented. Hence, mesoporous TiO₂ nanoparticle films (for example, commercial P25 nanoparticle) have been extensively studied as the photoanodes for QDSSCs and DSSCs, due to the appreciable internal surface area and good electron transport (Wang 2014).

Mesoporous structure is desired for TiO₂ wide band gap semiconductors to provide large surface area for absorption of more QDs in harvesting visible light efficiency. Therefore, TiO₂ is an attractive material for the solar cells' application because of its surface photochemistry, physical and chemical stability as semiconductor material. In addition, TiO₂ is an n-type semiconductor with wide band gap of 3.0 eV for rutile and 3.2 eV for anatase. The anatase is preferred for use in solar cells because of its higher mobility and catalytic properties. The conduction band, E_{cb}

of anatase TiO_2 is -4.21 with respect to absolute vacuum scale (AVS). So, it is otherwise called E_{cb} -4.21 eV versus vacuum. The wide band gap of bulk TiO_2 favours absorption of a portion of solar spectrum from ultraviolet down to ~ 400 nm. The mesoporous TiO_2 is coated with these QDs using colloidal QD or in situ fabrication and pre-synthesized QDs (also known as ex situ fabrication) (Liu & Kamat 1993, Emin et al. 2011).

The general structure of a QDSSC and its operation is depicted in Figure 1.3 (Jun et al., 2013). The working mechanism of the QDSSC is similar to that of the DSSC. When the QDs (CdSe) is subjected to band gap excitation, upon illumination, electron-hole pairs are formed in the QDs. The electrons will enter the conduction band (CB) of the QD and the hole remains in the valence band (VB). The excited QD injects the electron from its CB into the CB of the wide band gap semiconductor (TiO_2) and in doing so, it is itself oxidized with the hole remaining in the valence band. The injected electron from the QD percolates through the porous TiO_2 network and ultimately reaches the conducting glass. It then travels from there through the external load and completes the circuit by entering back through the counter electrode. The generated voltage is perceived as an evidence of the solar energy conversion to electric energy. This voltage corresponds to the difference between the quasi-Fermi level of the electron in the photoanode and the redox potential of the polysulfide electrolyte, which usually consists of a ($\text{S}^{2-}/\text{S}_x^{2-}$) redox couple. The oxidized QD is then restored (hole is filled with electron) when it is reduced by S^{2-} from the electrolyte and in turn it is oxidized into S_x^{2-} that diffuses to the counter electrode.

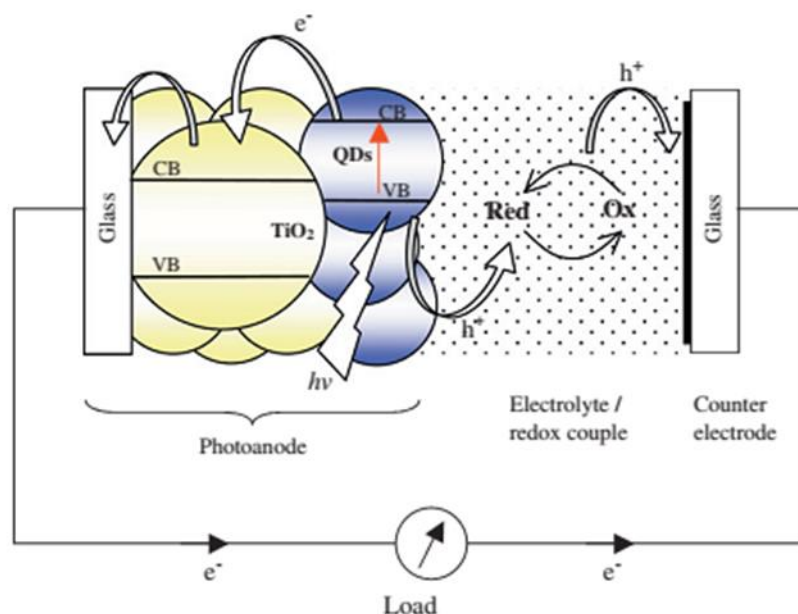


Figure 1.3 Structure and operating principle of a typical QDSSC (Jun et al., 2013).

1.2 Problem Statement

High coverage CdSe nanoparticles films can generate high power conversion efficiency in CdSe-sensitized QDSSCs. However, high coverage of CdSe nanoparticles films are difficult to be obtained in the absence of linkers. Several methods are available to obtain high coverage of films, but it is distinctly related to the nature of the nanoparticles synthesized and deposited on the substrates. Commonly, chemical bath deposition (CBD) (Choi et al. 2014), successive ionic layer adsorption and reaction (SILAR) (Emin et al. 2011), bifunctional molecular linkers (Song et al. 2012), and direct adsorption (DA) methods (Wang et al. 2017) are used for preparing quantum dots and attaching them to the wide band gap semiconductor material and substrate surfaces. However, the major drawbacks of the CBD and SILAR methods is the wastage of solution after every deposition. Other disadvantages of these methods include slow growth of particles form a film at the substrate surface, long deposition time, poly-disperse nanoparticles in solution and non-uniform coverage to substrate.

The bifunctional molecular linkers approach is equally limited by low repeatability due to the instability between quantum dot (QD) to linker, and linker to substrate interaction. On the other hand, the DA method often leads a high degree of QD aggregation and a low surface coverage when QDs are attached on the wide band gap semiconductor film (Lana-villarreal & Bisquet 2009). In contrast, the electrophoretic deposition (EPD) method has several desirable advantages. Specifically, the deposition time is short, it requires only simple apparatus, it allows easy control of the thickness and morphology of a deposited film, and there is strong adherent QD deposition onto the wide band gap semiconductor material and substrate surfaces.

Lee and co-workers investigated photovoltaic cells by electrophoretically depositing the CdSe nanoparticles on ZnO which yielded 0.5% power conversion efficiency (Lee et al. 2014). Chiang and co-workers investigated the preparation of photo-electrodes, where an aliquot of a commercial TiO₂ suspension was deposited onto the TCO by the EPD for DSSC. Conversion efficiency 0.04% was reportedly reproduced (Chiang et al. 2015). In another study by Salant et al. 2010a, electrophoretic deposition method was used to generate high power conversion efficiency in CdSe sensitized QDSSCs. Besides these, electrophoretic deposition (EPD) was previously employed to deposit semiconductor, metallic, and insulating nanoparticles on conductive substrates and polymers (Jia et al. 2008). Significantly, the deposited CdSe QDs adhered strongly both on negative and positive electrodes (Islam et al. 2004). Rosenthal and co-workers fabricated photovoltaic cells by EPD of CdSe nanocrystals on flat TiO₂, yielding low conversion efficiencies, while Islam and co-workers studied the smooth and robust films of CdSe nanocrystals by EPD method (Islam et al. 2004). For QDSSC application, Salant and co-workers fabricated CdSe nanoparticles deposited on TiO₂ by EPD method and their efficiency value is 1.7% (Salant *et al.*,

2010b). Likewise, Kumar and co-workers studied the functionalized electrophoretic deposition of CdSe quantum dots onto TiO₂ electrode for QDSSC, which yielded an efficiency of 0.16% (Kumar 2012). On the other hand, Zarazúa and co-workers stated EPD significantly decreased the Au NPs deposition times to TiO₂ layer (Zarazúa et al. 2016). Generally, several different types of QDs have been deposited using EPD, including CdSe (Smith et al. 2009), CdTe, PbS, and PbSeS (Benekohal et al. 2012), CdSSe (Santra & Kamat 2012), CdSeTe (Esparza et al. 2017), CuInS₂ (Sensitized et al. 2013), CuInS₂/ZnS (Liu et al. 2019), and CdSe/CdS nanorods (Salant et al. 2012).

This work aims to show that the EPD on the TiO₂ electrodes indeed provides a driving force leading to highly effective QD deposition on the mesoporous TiO₂ surface. It is known that the EPD method has the advantage of obtaining better CdSe QDs deposition onto TiO₂ layers with reduced deposition time and it can facilitate easier deposition. Hence, this study aims to use EPD method not only to fabricate the photoanode CdSe/TiO₂ but also to study the effect of the mixed CdSe-TiO₂ nanoparticles. The efficiency of optimized photoanode CdSe/TiO₂ is increased in this study. So far, the combination of CdSe and TiO₂ has not been experimented by researchers to make the QDSSC. Although, mixing the CdSe and TiO₂ can facilitate better contact between CdSe and TiO₂ which can in turn improve the performance of the solar cell. However, the problem with this system is that photoexcited electrons need to travel a long pathway (the thickness of TiO₂) before it reaches the conductive substrate, where the photoexcited electron is susceptible to recombination with the sub-band gap state of TiO₂. Mixed CdSe-TiO₂ photoanodes will create efficient electron injection from CdSe conduction band to the TiO₂ electrode effectively, to reduce the recombination and improve the efficiency. A novel attempt to mix CdSe-TiO₂ nanoparticles deposit on FTO substrates may produce positive results.

1.3 Research Objectives

The principal objectives of this research are:

- i. To synthesize and evaluate the CdSe nanoparticles with different amounts of TOPO and TiO₂ nanoparticles in chloroform for EPD method.
- ii. To investigate the electrophoretic deposition (EPD) of CdSe nanoparticles, TiO₂ nanoparticles and mixed CdSe-TiO₂ nanoparticles on FTO glass substrate.
- iii. To evaluate the performance of QDSSC with optimum photoanode.

1.4 Research Scope

This research study aims to explore the use of CdSe and TiO₂ for fabrication of photoanodes for QDSSC application. The role of amount of TOPO and the purification process in synthesizing high-efficient nanoparticles for enhanced deposition on the FTO substrate. The CdSe and TiO₂ nanoparticles were prepared in chloroform. In this research, the behaviour of synthesized nanoparticles such as TiO₂ and CdSe for different amounts of TOPO which acts as a capping ligand. TOPO capped CdSe nanoparticles are soluble in chloroform however, TOPO has incompatibility issues when applied for EPD method. The preparation of TiO₂ in polar and aqueous solvents is also explored. The most suitable method to synthesize TiO₂ in chloroform would be established. Furthermore, the possibility of performing layer by layer deposition and co-deposition of CdSe and TiO₂ has been investigated. A series of experiments were carried out using the EPD process of CdSe, TiO₂ and mixed CdSe and TiO₂. In an attempt to identify and determine the effect of different EPD parameters on the deposition thickness, parameters like applied voltage, deposition

time, electrode gap and volume of CdSe and concentration of TiO₂ were varied and studied. The fabricated CdSe/TiO₂ and CdSe-TiO₂ films were used as photoanodes, Cu₂S as a counter electrode and polysulfide electrolyte in QDSSC, and the performance of the fabricated QDSSC was studied using J-V and EIS measurements.

1.5 Organization of Thesis

The thesis was organized in five chapters. The brief summary on the chapters are described as follows:

- a) Chapter One includes a brief introduction about the research study, problem statements, objectives, and the scope of this research work.
- b) In Chapter Two, a comprehensive review of literature on the formation, synthesis methods and electrophoretic deposition methods, properties for CdSe and TiO₂ is presented. The fundamentals forming the basis for EPD applications are also discussed in detail. Also, the working principle of QDSSC for the photoanode, photocathode and the electrolyte are included.
- c) Chapter Three details the information about raw materials used in this study, the experimental design and the methods and procedures followed to deposit CdSe and TiO₂ by EPD method. A brief explanation on the characterization techniques of CdSe/TiO₂ and mixed CdSe-TiO₂ films is also described.
- d) Chapter Four presents the experimental results and a thorough discussion on the formation behaviour of different TOPO amounts in CdSe nanoparticles solution. The effect of the EPD parameters on the deposition characteristics for deposition of CdSe, TiO₂ and mixed CdSe and TiO₂ films have been elucidated. Different characterization methods were adopted to examine and evaluate the

behaviour of the deposited coatings, which is comprehensively analyzed in this section.

- e) Chapter Five summarizes the findings and provides the directions and suggestions for further studies on this work.

CHAPTER 2

LITERATURE REVIEW

2.1 Introduction

QDs are categorized as smaller than nano semiconductor particles. In general, particles with sizes between 1-100 nm are regarded as nanoparticles. They act as a path between bulk materials and atomic or molecular structures. QDs composed of tiny semiconductor particles of a few nano meters size, having optical and electronic properties that differ from those of larger light-emitting diode (LED) particles. Their optoelectronic properties change as a function of both size and shape (Kagan *et al.*, 2000). Larger diameter QDs (5–6 nm) emit longer wavelengths, with different colour emission such as orange or red. Meanwhile, smaller diameter QDs (2–3 nm) emit shorter wavelengths, yielding colours of either blue or green, although the specific colour and size vary depending on synthesized temperature and reaction time to get the desired nanoparticle size. Figure 2.1 shows the colour change with different sizes of nanoparticles depending on synthesized temperature and reaction time under UV-irradiation (blue fluorescence colour is 2.1 nm at 110 °C for 40 min, dark-green fluorescence colour is 2.4 nm at 120 °C for 50 min, yellow-green fluorescence colour is 2.7 nm at 150 °C for 60 min, yellow fluorescence colour is 3.0 nm at 190 °C for 80 min, orange fluorescence colour is 3.7 nm at 220 °C for 100 min, red fluorescence colour is 4.3 nm at 250 °C for 120 min) that the size values were calculated from the absorbance spectra, according the equation of (Yu et al. 2003).

Chalcogenide nanoparticles such as CdSe, CdS, CdTe and etc. are commonly used as quantum dots (QDs) sensitizers in electronic application. Cadmium selenide (CdSe) nanoparticles (QDs) have been received an increasing attention for quantum dots sensitized solar cell (QDSSC) application due to their exceptional optical

properties, ease of fabrication, tunability of band gap energy, narrow emission spectrum, good photo stability, broad excitation spectra, high extinction coefficient and multiple exciton generation. CdSe is an inorganic compound and it is classified as an II-VI semiconductor of the n-type. CdSe absorbs photon efficiently because its absorption wavelength is in the visible range and the band gap value of a CdSe is 1.73 eV (Peter 2011). The conventional applications of CdSe are for transparent to infra-red (IR) light and pose limitation in photo resistors and windows applications for instruments utilizing IR light.

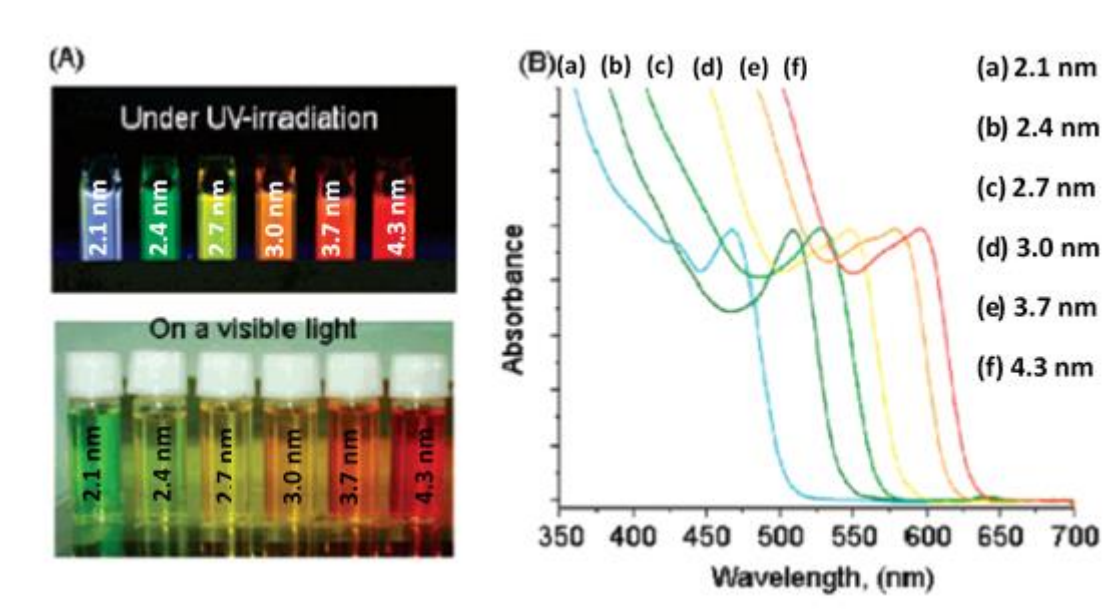


Figure 2.1 Different sizes CdSe quantum dots, synthesized at a slow-increasing temperature gradient with different color light emissions (A) images under UV irradiation and on visible light (B) normalized absorbance spectra (Zlateva et al., 2007).

2.2 CdSe Nanoparticles

2.2.1 Properties of CdSe Nanoparticles

CdSe is an inorganic compound and it is classified as an II-VI semiconductor of the n-type. CdSe nanoparticles possess wurtzite (hexagonal) and zinc blende (cubic)

structures. They promote excellent opto-electronic properties. The physical and chemical properties of CdSe nanoparticles are size-dependent. While synthesizing semiconductor nanoparticles, the deposition parameters can be varied in order to control the size of the nanoparticles (Mastai et al., 1999). By altering the particle size, the band gap can be changed further to match a desired band gap range. It is critical to understand the physical and chemical characteristics of the CdSe nanoparticles for a better research focus. The energy level diagram of CdSe nanoparticles is presented in Figure 2.2 (Vinitha & Divya 2018). When the absorbance wavelength of CdSe increases, its particle size will also increase while the band gap value decreases. CdSe absorbs photon in the visible range of ~ 700 nm efficiently since the band gap value of CdSe is 1.73 eV (Peter, 2011). CdSe has attracted a great amount of attention in the QDSSC research due to its advantages such as ease of fabrication, tunability of band gap energy, narrow emission spectrum, good photostability, broad excitation spectra, high extinction coefficient and multiple exciton generation (William & Yu et al., 2003).

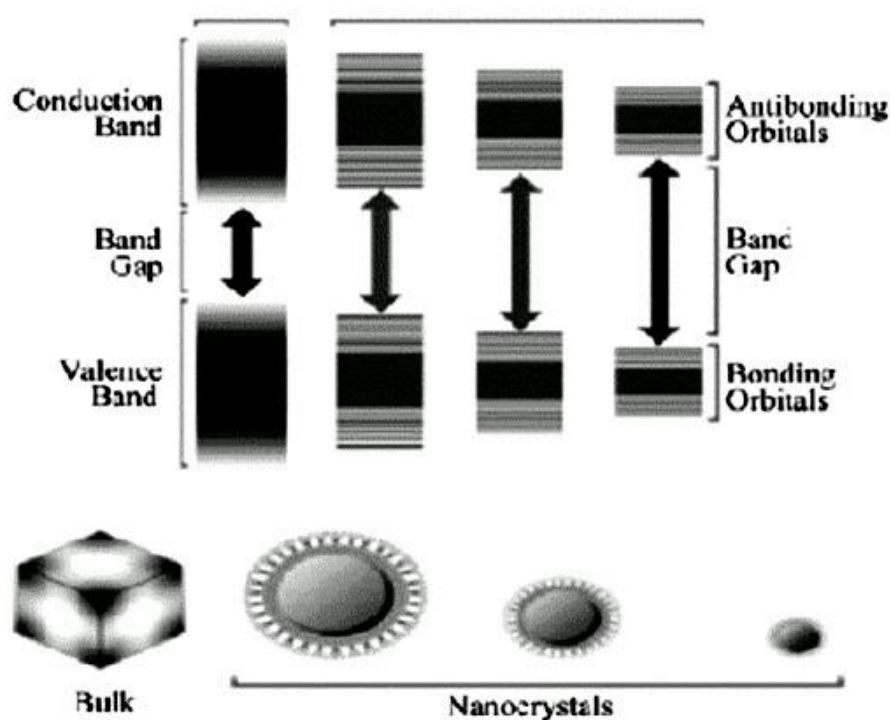


Figure 2.2 Energy level diagram of CdSe nanoparticles (Vinitha & Divya, 2018).

2.2.2 Synthesis of CdSe Nanoparticles

Murray, Morris and Bawendi had proposed a synthesis of CdSe nanoparticles in which the main concept is based on the pyrolysis of organometallic reagents by firstly injecting them into a hot coordinating solvent (Murray et al., 1993). Murray and co-workers used dimethylcadmium $(\text{CH}_3)_2\text{Cd}$ as the organometallic precursors while trioctylphosphine oxide (TOPO) as the hot coordinating solvent operating at 300°C . TOPO was chosen as the coordinating solvent since TOPO has a high boiling point and enables reaction to take place above the nucleation temperature. Besides, TOPO allows nanoparticles to be soluble in organic solvents and prevents agglomeration. Peng & Peng (2001) reported that impurity such as phosphonic acid presents in TOPO, which leads to a fluctuation in the synthesis of CdSe nanoparticles. Furthermore, dimethylcadmium $(\text{CH}_3)_2\text{Cd}$ is very toxic, unstable at room temperature and air-sensitive which required this method to be modified as suggested by Qu & Peng (2002). In order to solve this problem, they had suggested to synthesize CdSe QDs by replacing dimethylcadmium $(\text{CH}_3)_2\text{Cd}$ with cadmium acetate $\text{Cd}(\text{CH}_3\text{CO}_2)_2$ (Mekis et al., 2003), cadmium carbonate (CdCO_3) (Qu et al., 2001) or cadmium oxide (CdO) (Peng & Peng, 2001). Co-solvent such as tetradecylphosphonic acid (TDPA) is added to supplement the unknown impurity and slow the nucleation process so that the size distribution is not distorted when the system cools to the growth temperature (Qu & Peng 2002). Besides, the use of TDPA can also help to produce large batches of nanoparticles with a narrow dispersity as larger volumes of reagents can be nucleated. The second co-solvent, hexadecylamine (HDA) can also be added to provide resistance towards Ostwald ripening. The use of TOPO/TDPA/HDA help in maintaining a narrow dispersity of nanoparticles up to seven hours at growth temperature whereas the use of

only TOPO and TDPA yields a major broadening of the band edge absorption and large polydispersity in less than an hour (Rosenthal et al., 2007).

2.2.3 Growth Mechanism of CdSe Nanoparticles during Synthesis

Precursors of Cd and Se coordinated in trioctylphosphine (TOP) are normally kept at a temperature below the reaction threshold before injection into the pre-heated TOPO matrix. The matrix serves to engulf the precursor droplets and promotes the subsequent chemical reaction into it between the Cd and Se ions forming seeds of nanoparticles. Figure 2.3 shows the growth of the CdSe nanoparticles with addition of coordinated Cd and Se ions on the surface with Cd bounds to TOPO and Se bounds to TOP. Hot injection leads to an instantaneous nucleation, quenched by fast cooling of the reaction mixture and because supersaturation is relieved by the nucleation burst. In 1950, La Mer and Dinegar had found that the production of monodispersed colloids requires a temporarily discrete nucleation event followed by a slower controlled growth of the existing nuclei (Donegu et al., 2005 and Geissbühler, 2005).

In the synthesis of quantum dots, the two common events that will occur are the nucleation process in which precursors at a higher temperature will decompose to form a supersaturated monomer followed by a burst of nucleation and growth of this nuclei from molecular precursor. The synthesis begins with the rapid injection of organometallic reagents into hot coordinating solvent to produce a discrete homogeneous nucleation. Then, further nucleation is prevented when depletion of reagents through nucleation and sudden temperature drop occur. Crystallites growth will continue when reheating is applied on the solution. At this stage, the crystallites growth appears to be consistent with Ostwald ripening is where small crystallites which less stable were dissolved into the large crystallites. Therefore, the size of crystallites is

dependent on the reaction time in which larger particles will be formed when the reaction time is longer, and relatively small nanoparticles will be produced when the reaction time is shorter. Figure 2.4 shows the growth and nucleation of quantum dots based on the La Mer model (Farkhani and Valizadeh, 2014).

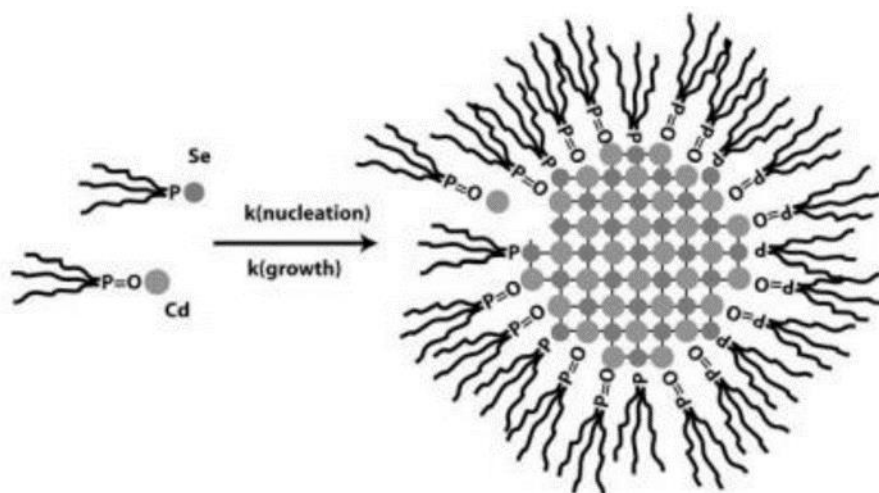


Figure 2.3 Growth of CdSe nanoparticles onto TOPO matrix (Geissbühler, 2005).

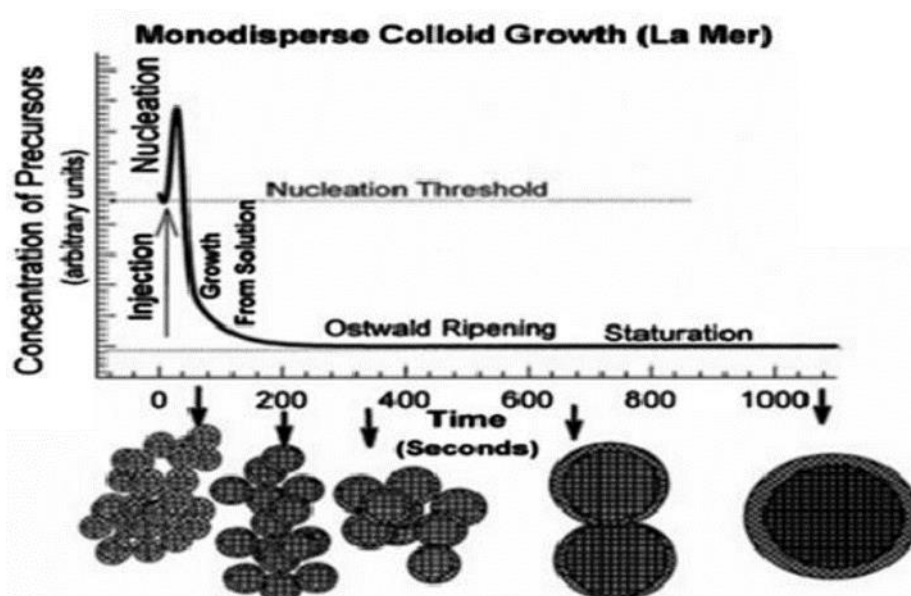


Figure 2.4 Stages of growth and nucleation of quantum dots based on La Mer model (Farkhani and Valizadeh, 2014).

2.2.4 TOPO Ligand

CdSe nanoparticles are prepared as colloidal suspension and quenched in solvent in order to control the growth of the CdSe nanoparticles. Organic ligands are frequently used as the capping ligand in the production of quantum dots such as those consisting of CdSe. These ligands can prevent oxidation and stabilize nanoparticles in solution as shown in Figure 2.5. Hydrophobic ligands such as tri-octyl phosphine (TOP) and tri-octyl phosphine oxide (TOPO) cannot absorb water (Aldana et al. 2001) while hydrophilic ligands such as mercaptopropionic acid (MPA) and mercaptoundecanoic acid (MUA) in contrast can absorb water (Schultz et al., 1997).

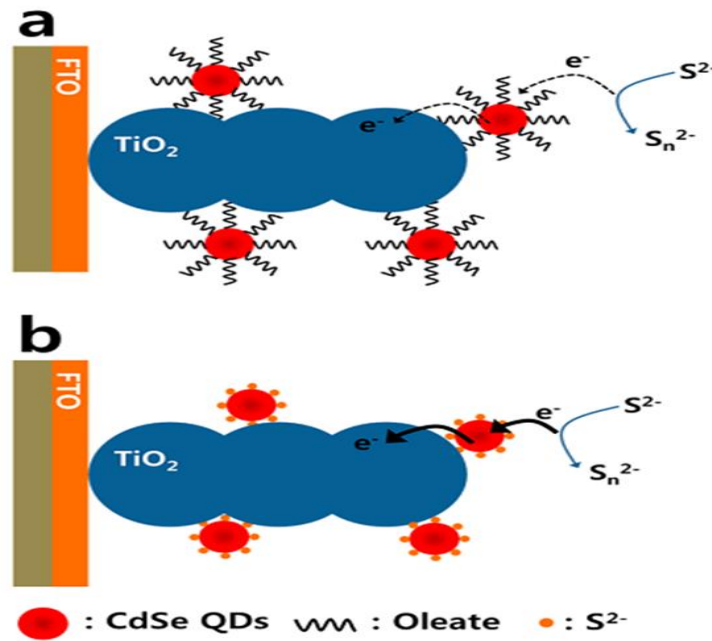


Figure 2.5 Schematic diagram of charge transferring at the interfacial region in QDSSC based on colloidal CdSe QDs capped by (a) long organic chain, oleate; and (b) atomic level inorganic ligand, S²⁻ (Yun et al., 2014).

Wu et al., (2005) described that the capping ligands; tri-octylphosphine oxide (TOPO), hexadecyl hexadecanoate (HH) and benzophenone (BP) were used for the synthesis of high-quality CdSe nanocrystals. TOPO appears to play an important role in the preparation of monodisperse CdSe nanoparticles. CdSe nanoparticles nucleate and grow rapidly in the presence of TOPO, reaching a limiting diameter of 5 nm within

approximately 1 min. Only a small amount of TOPO (3% or less of the reaction mixture) is required to achieve a narrow particle size distribution. Zhen et al., (2009) reported that TOPO is used as the capping ligand in the preparation of CdSe nanowires. The organic capping ligands; TOPO is also used in the colloidal synthesis of CdSe nanorods. The length of the organic capping ligand has a profound effect on the growth kinetics of colloidal CdSe nanorods and the stability of the nanorod solution. By results, the shorter the alkylphosphonic acid ligand, the more elongated and more branching are the nanorods. When mixtures of alkylphosphonic acids are used, higher molar fraction of the shorter ligand produces more elongated and branched nanorods (Wang et al., 2007).

In this thesis, different amount of TOPO was used in the synthesis of CdSe nanoparticles. In this case, TOPO served the synthesis by solubilizing the growing CdSe nanoparticles. CdSe is unlikely to escape from TOPO capping as well as being deposited in the EPD process due to the long ligand TOPO structure. However, in few cases, only TOPO can be deposited instead of CdSe nanoparticles. This condition can cause disturbance in the EPD process.

2.2.5 Optical Properties of CdSe Nanoparticles

The synthesis of different sizes of CdSe nanoparticles can be identified using the UV-vis spectroscopy. The size of CdSe quantum dots is controlled by the time of growth of CdSe nanoparticles before quenching in toluene. The size of CdSe QDs is determined the wavelength from UV-vis spectroscopy. Figure 2.6 (Yuan and Krüger, 2011) shows the UV-vis spectra and photoluminescence spectra of different sized CdSe QDs, in which a shorter wavelength corresponds to a small particle size and a longer wavelength corresponds to a big particle size. These quantum dots of different sizes can

emit light of different color due to the quantum confinement effect. Bigger quantum dots give lower energy fluorescence, which is possible to emit red light whereas smaller quantum dots emit blue light. This shows that the light coloration is directly related to the energy levels of the quantum dots while the size of the quantum dots is inversely proportional to the energy band gap. Therefore, larger quantum dots have more energy level but with lower band gap energy, which are more closely spaced. This can allow larger quantum dots to absorb photons by consuming less energy (Mahajan, 2013).

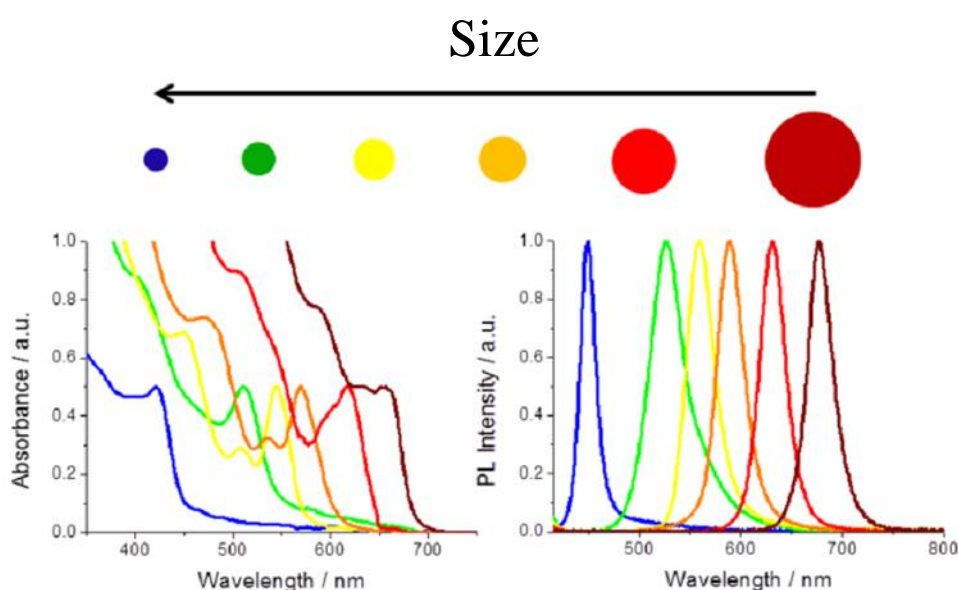


Figure 2.6 Absorption spectra and photoluminescence spectra of different sized CdSe quantum dots (Yuan and Krüger, 2011).

2.2.6 Purification of CdSe Nanoparticles Solution

Knowledge on the distribution of ligands in the QD organic system after purification process is critical in predicting and interpreting the structural, electronic, and optical properties of solutions and films of QDs. This distribution is dependent on the strength of the respective QD ligand interactions and the relative solubility of the ligands in the solvent system. Morris-Cohen et al., (2010) purified QDs by using 5 ml

of chloroform (ACS grade, VWR) with 10 ml of methanol (ACS grade, VWR) and isolated an orange pellet through centrifugation at 3500 rpm for 5 minutes.

CdSe QDs synthesized with TOPO contain nominal surfactants such as TOPO, TDPA, HDA and TOP including 10 different phosphorus-containing impurities such as n-octylphosphonic acid (OPA). Figure 2.7 shows the chemical structure of the ligands present in a QD organic system. Morris-Cohen et al., (2010) found that in L-type ligands, HDA, TOPO and TOPSe are present in both bound and unbound states whereas in X-type ligands, OPA, PPA and stearate are bounded to the surface of QDs. Hence, the purpose of a purification process is to remove the excess ligands such as TOPO, TDPA, HDA and TOP from the synthesis process of CdSe (Morris-Cohen et al., 2010). The methanol and CdSe solution the nanoparticles were precipitated and isolated by centrifugation. After centrifugation two layers of solution form with the colourless solution on top and the CdSe powder in the bottom. The colourless solution was poured out and the CdSe powder re-dispersed in chloroform or toluene which the purification is done completely using methanol for CdSe QDs that capped by TOPO. During purification process, methanol is used as the flocculating agent because it is miscible with toluene and can readily dissolve the bound ligands. Murray et al., (1993) proposed that quantum dots agglomeration is induced by Van der Waals forces, in which the capping agents will leave the quantum dots surface and dissolving within the methanol-toluene mixture and results in aggregation. Subsequently, Jia et al., (2008) investigated that the smoothest films can be deposited when the nanocrystals are washed two or three times before electrophoretic deposition. However, they claimed that if nanoparticles are washed more than three times, then rough and clumpy films will be produced (Jia et al., 2008). Figure 2.8 displays that as purification process continues, the L-type ligands are being removed from the system while the X-type ligands are unchanged throughout